14th Australasian Fluid Mechanics Conference
Adelaide University, Adelaide, Australia
10-14 December 2001

Incipient Motion of Bivalve Shells on Sand Beds under Currents

Subhasish Dey[1]
[1]**Department of Civil Engineering**
Indian Institute of Technology, Kharagpur 721302, West Bengal, INDIA

Abstract
Hydrodynamic forces on a solitary bivalve shell, resting over a sand bed, are analyzed to determine the critical shear stress for the condition of incipient motion including the effect of turbulent fluctuations. Three types of shells, namely Coquina Clam, Cross-barred Chione and Ponderous Ark, were tested experimentally for the condition of incipient motion. The results obtained using the present model agree satisfactorily with the experimental data.

Introduction
Various types of bivalve shells are deposited in biologically productive coastal regions encompassing the surf zone, tidal entrance and estuarine waters near the entrances. The beach at John o'Groats in Scotland is one of the examples of a beach exclusively composed of about 97% of the surficial sedimentary material as shells. A matrix of shell debris is also found in Southern Gulf Coast of Florida in USA and the banks of Lower Medway estuary in England.

The shell halves of a live bivalve shell being almost like a mirror image are joined at a tip known as umbo. When shells die, the shell halves are eventually separated out by the action of flow of water over a period of time. Thus, most of the coastal sedimentary material consists of the separated halves of shells. Little is known about the transport of shells under the flow of water, as no attempt has so far been made to determine the movement of shells by the action of flow. In this study, the incipient motion of shells on a horizontal sand bed, under a unidirectional flow of water, is investigated theoretically and experimentally for some commonly available species of bivalve shells, namely Coquina Clam, Cross-barred Chione and Ponderous Ark.

Shape Parameters
The irregular shaped particles are usually defined by the Corey shape factor *SF* as

$$SF = c/\sqrt{ab} \tag{1}$$

where *a*, *b* and *c* = longest, intermediate and smallest dimensions of particle along three mutually perpendicular axes, respectively. The main drawback of using *SF* is that it does not account the distribution of the surface area and the volume of the particle. To overcome this difficulty, Alger and Simons [1] proposed a new shape parameter β given by

$$\beta = SF(d_s/d_n) \tag{2}$$

where d_s = area diameter, that is the diameter of a sphere having the same surface area as that of the particle; and d_n = nominal diameter, that is the diameter of a sphere having the same volume as that of the particle. Thus, d_s and d_n are given by

$$d_s = \sqrt{s/\pi} \tag{3}$$

$$d_n = \sqrt[3]{6v/\pi} \tag{4}$$

where *S* = total surface area; and *v* = volume.

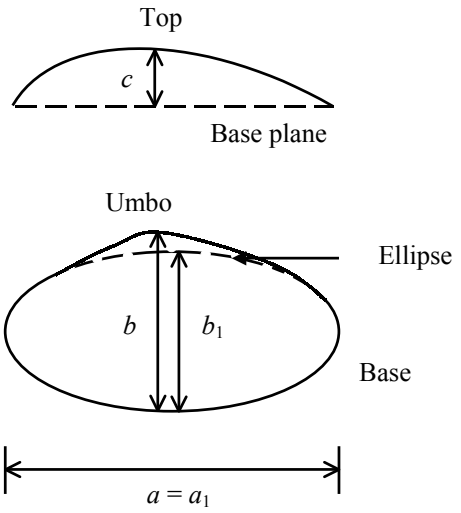

Figure 1. Shape of bivalve shell and its dimensions along three mutually perpendicular axes.

Figure 1 shows the dimensions *a*, *b* and *c* of a bivalve shell. Its base can be considered as an ellipse having major and minor axes a_1 and b_1, respectively. The base area A_s of a shell is approximated by that of an ellipse, as was done by Mehta et al. [8]. It is

$$A_s = 0.25\alpha_1\pi a_1 b_1 \tag{5}$$

where α_1 = area shape factor. As *b* usually passes through the umbonal region, b_1 can be represented introducing a new shape factor α_2 as $b_1 = \alpha_2 b$. It is also observed that a_1 is equaling *a*. Therefore, the base area A_s is given by

$$A_s = 0.25\alpha_1\alpha_2\pi ab \tag{6}$$

The total surface area *S* is related to the base area A_s as

$$A_s = 0.5\alpha_3 S \tag{7}$$

where α_3 = factor. Using (1) - (7), the shape parameter β and area diameter d_s are expressed as

$$\beta = 0.57c\sqrt{\alpha_4}/\sqrt[3]{v} \tag{8}$$

$$d_s = 0.707\sqrt{\alpha_4 ab} \tag{9}$$

where $\alpha_4 = \alpha_1\alpha_2/\alpha_3$.

Preparation of Samples of Shells
Three types of bivalve shells, namely Coquina Clam, Cross-barred Chione and Ponderous Ark, shown in Figure 2 were used for the testing. The relative density *s* of a particular type of shell was determined. Each shell was weighed and numbered for proper identification. The volume of shell *v* was determined from $m/s\rho$, where *m* is the mass of shell and ρ is the mass density of

water. The factors α_1 and α_2 occur as a product $\alpha_1\alpha_2$ in (6) being considered as a single shape factor. The factor $\alpha_1\alpha_2$ was estimated using a, b and A_s. The base area A_s was measured by using a plan-meter. Furthermore, it is not appropriate to use α_3 and α_4 separately, as α_3 occurs in (8) and (9) through α_4 (= $\alpha_1\alpha_2/\alpha_3$). However, α_3 was obtained from (7), using the known S, which was obtained from $S = 2v/t_c$. Here, t_c is the thickness of the shell that was measured at the origin of the three mutually perpendicular axes. This was verified from some samples, for which S was determined by dividing the shell surface into a number of trapezoidal subareas.

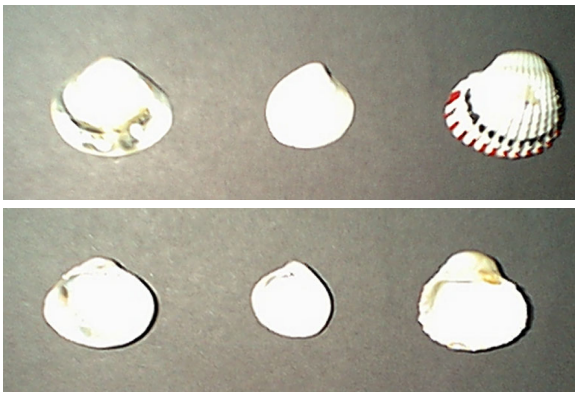

Figure 2. Selected samples of bivalve shells from left to right: Coquina Clam, Cross-barred Chione, and Ponderous Ark.

Experimental Set-up and Procedure

Experiments were conducted in a rectangular flume of 0.075 m wide, 0.25 m deep and 5 m long. The sand particles of an appropriate size were glued on the surface of the floor in order to simulate the roughness. Two sizes of sands, having mean diameters d = 0.80 mm and 0.30 mm, were used for creating the bed roughness. Before starting an experimental run, the shell with umbo downstream position was placed, at the middle of the sand bed, 3.5 m downstream the inlet of the flume in order to get a fully developed flow. Water was introduced to the set-up by gradually opening a valve in the upstream and the discharge was adjusted so that the incipient condition was reached when the shell started moving on the sand bed. An important feature of shell movement was noticed in the experiments. When the shell was placed with umbo upstream or sidewise position, the shell spun by the action of flow velocity to become umbo downstream position and moved in the streamwise direction. The main cause of spinning motion is attributed to the fact that a turning moment was induced due to the unbalanced hydrodynamic force as the umbo is always eccentric to either of the side of the shells. This is regarded as unstable condition. However, the shell with umbo downstream position moves under lower flow velocity without any spin being the case for incipient motion. Once the incipient condition was reached, the discharge Q and the corresponding flow depth h were registered. The flow depth h is a distance from the free surface of flow to the virtual bed level. The virtual bed level was considered at $0.25d$ below the top level of the bed particles, as was done by Dey [2] and Dey et al. [6]. Here, d is the mean sand diameter. The angle of friction ϕ between shell and sand bed was determined by tilting the flume, keeping a shell on the rough bed of the flume in submerged condition, until the shell just started to move.

Estimation of Bed Shear Stress

The equation of bed shear stress τ_b as a function of dynamic pressure is used here. It is

$$\tau_b = 0.125 f_b \rho V_b^2 \tag{10}$$

where f = friction factor; and V = mean velocity of flow. Subscript b refers to the quantities associated with the bed. The Colebrook-White equation, used to evaluate f_b, is given below:

$$\frac{1}{\sqrt{f_b}} = -0.86 \ln\left(\frac{k_s P_b}{14.8 A_b} + \frac{2.51}{R_b\sqrt{f_b}}\right) \tag{11}$$

where k_s = equivalent sand roughness; A = flow area; P = wetted perimeter; and R = Reynolds number of flow. In the present study, the bed is rough and the side-walls are smooth. As a result of which, f_w is considerably different from f_b; where subscript w refers to the quantities associated with the side-walls. Consequently, τ_w is significantly different from τ_b. Therefore, Vanoni's [9] method of *side-wall correction* for a rectangular flume is used here (also available in Dey and Debnath [4,5]).

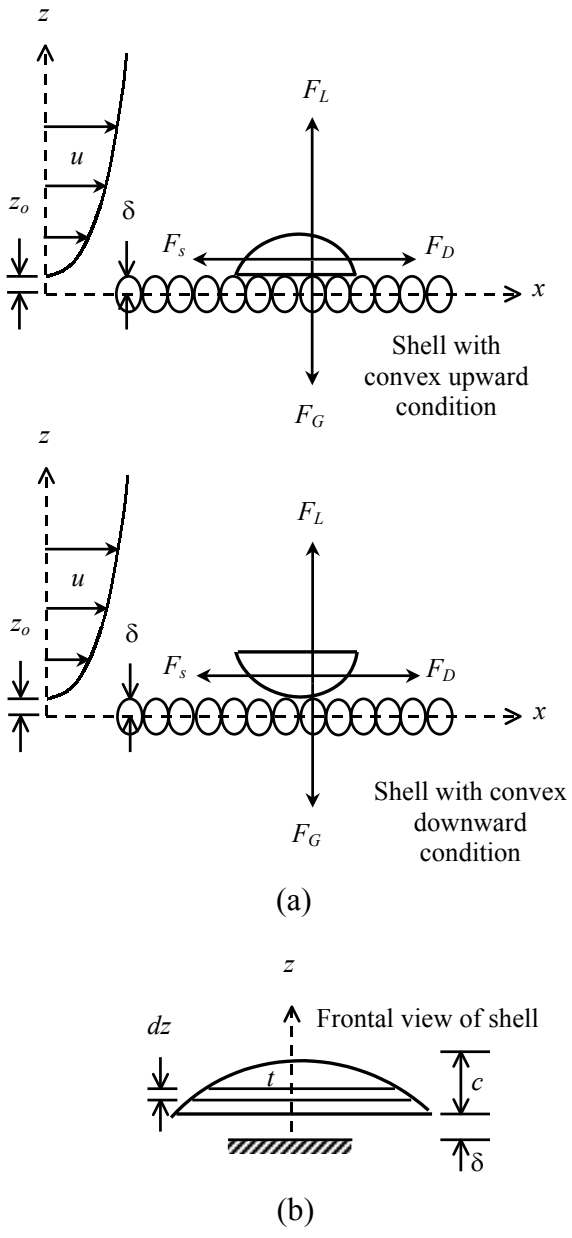

Figure 3. Definition sketch: (a) Schematic presentation of forces acting on a shell in convex upward and downward conditions; and (b) frontal area of a shell in convex upward condition.

Forces Acting on a Shell

In a unidirectional flow, the force acting on a shell in convex upward and downward conditions placed on a horizontal sand bed is shown in Figure 3(a). The forces are the downward force due to its submerged weight (F_G) and the hydrodynamic force, being resolved into drag force (F_D) and lift force (F_L). When the shell is about to move downstream from its original position, the equation of force balance is

$$F_s = F_D \tag{12}$$

where F_s = static Coulomb friction force between shell and sand bed. The static Coulomb friction force is given by

$$F_s = (F_G - F_L)\mu_c \tag{13}$$

where μ_c = static Coulomb friction factor = tanϕ. Equating (12) and (13), one gets

$$F_D = (F_G - F_L)\tan\phi \tag{14}$$

Using (8), the submerged weight of the shell is given by

$$F_G = v(s-1)\rho g = 0.185(s-1)\rho g c^3 \alpha_4^{1.5}/\beta^3 \tag{15}$$

where g = gravitational constant. The drag force F_D is given as

$$F_D = 0.5 C_D \rho u_m^2 A_p \tag{16}$$

where C_D = drag coefficient; u_m = mean flow velocity received by the frontal area of shell; and A_p = frontal area of shell. The view of shell in convex upward condition [Figure 3(a)] is similar to a car, whose value of C_D being 0.45 is used here. On the other hand, the value of C_D in convex upward condition considered 0.54 gives reasonable results. The frontal area A_p with umbo downstream position is approximated by a segment of circular arc having height c and chord length a. It is

$$A_p = 0.25c^2(0.25\hat{a}^2 + 1)^2 \xi \tag{17}$$

where $\hat{a} = a/c$; and

$$\xi = \arccos\left(\frac{\hat{a}^2 - 4}{\hat{a}^2 + 4}\right) - 4\hat{a}\frac{\hat{a}^2 - 4}{(\hat{a}^2 + 4)^2} \tag{18}$$

The lift force F_L, caused by the shear flow, is as follows:

$$F_L = 0.5 C_L \rho u_m^2 A_s \tag{19}$$

where C_L = lift coefficient. The base area A_s is obtained from (6).

Equation of Incipient Motion

Using (15) - (19) into (14), the equation of incipient motion of shells on a horizontal bed in normalized form is obtained as

$$\hat{\tau}_o = \frac{0.37\alpha_4^{1.5}\tan\phi}{C_D\beta^3\hat{u}_m^2\hat{k}_s\hat{A}_p(1+\lambda\tan\phi)} \tag{20}$$

where $\hat{\tau}_o$ = normalized time-averaged critical shear stress, that is $u_*^2/\Delta g k_s$ or $\tau_b/\Delta g\rho k_s$; u_* = time-averaged shear velocity, that is $(\tau_b/\rho)^{0.5}$; $\Delta = s - 1$; $\hat{u}_m = u_m/u_*$; $\hat{k}_s = k_s/c$; $\hat{A}_p = A_p/c^2$; and $\lambda = F_L/F_D$, that is $C_L A_s/(C_D A_p)$. The incipient motion over a sand bed is controlled by the applied instantaneous shear stress (fluctuating forces) at the bed [3,7]. The most important event for incipient motion is the sweep event, which has a dominant role in mobility of the particles at the bed. The sweep event applies shear in the direction of flow and provides additional forces to the viscous shear stress. Keshavarzy and Ball [7] reported that the magnitude of instantaneous shear stress in sweep event is much larger than time-averaged shear stress. Thus, they gave following equation:

$$u_{*t} = (1 + p\sqrt{\alpha - 1}\cos\psi)\, u_* \tag{21}$$

where u_{*t} = total shear velocity (= $u_* + u_t$); u_t = instantaneous shear velocity (= $u_* p\sqrt{\alpha-1}\cos\psi$ or $\sqrt{\tau_t/\rho}$); τ_t = instantaneous shear stress; p = probability of occurring sweep event; $\alpha = \tau_t/\tau_b$; and ψ = sweep angle. Therefore, incorporating the influence of instantaneous shear stress, (20) can be modified as

$$\hat{\tau} = \frac{0.37\alpha_4^{1.5}\tan\phi}{C_D\beta^3\hat{u}_m^2\hat{k}_s\hat{A}_p(1+\lambda\tan\phi)(1+p\sqrt{\alpha-1}\cos\psi)^2} \tag{22}$$

Keshavarzy and Ball [7] observed from the experimental data that the frequency of sweep events and the sweep angle ψ are 30 percent and 22°, respectively, for a region close to the bed. They also reported that $\tau_t \approx 1.4\tau_b$ near the bed.

Determination of $\hat{u}_m$

The frontal area of the shell with umbo downstream position is shown in Figure 3(b). The mean velocity of flow received by the frontal area of the shell is given by

$$u_m = \frac{1}{A_p}\int_{\varepsilon}^{c+\delta} t u\, dz \tag{23}$$

where t = frontal width of the shell at z with umbo downstream position; δ = normal distance between top of the bed particle and the virtual bed level, that is ζd; ζ = a factor; and ε = normal distance between the bottom or zero-velocity level of the shell and the virtual bed level. Here, ζ = 0.25 is considered, as was done by Dey [2]. The width t in Figure 3(b) is

$$t = 2c\sqrt{(1+\zeta\hat{d}-\hat{z})(0.25\hat{a}^2 - \zeta\hat{d} + \hat{z})} \quad \text{convex upward} \tag{24a}$$

$$t = 2c\sqrt{(\hat{z}-\zeta\hat{d})(0.25\hat{a}^2 + 1 + \zeta\hat{d} - \hat{z})} \quad \text{convex downward} \tag{24b}$$

where $\hat{d} = d/c$; and $\hat{z} = z/c$. The normalized velocity distribution over a sand bed in completely rough regime is

$$\hat{u} = (1/k)\ln(\hat{z}/\hat{z}_o) \tag{25}$$

where $\hat{u} = u/u_*$; k = von Karman constant (= 0.4); $\hat{z}_o = z_o/c$; and z_o = zero-velocity level above the virtual bed level (= $0.033k_s$). In this study, k_s is assumed as d, as was done by Dey [2]. The equations of $\hat{u}_m$, derived using (24a), (24b) and (25) into (23), are

$$\hat{u}_m = \frac{5}{\hat{A}_p}\int_{\hat{\varepsilon}}^{1+\zeta\hat{d}} \sqrt{(1+\zeta\hat{d}-\hat{z})(0.25\hat{a}^2 - \zeta\hat{d} + \hat{z})}\ln\left(\frac{\hat{z}}{\hat{z}_o}\right)d\hat{z}$$

for convex upward (26a)

$$\hat{u}_m = \frac{5}{\hat{A}_p}\int_{\hat{\varepsilon}}^{1+\zeta\hat{d}} \sqrt{(\hat{z}-\zeta\hat{d})(0.25\hat{a}^2+1+\zeta\hat{d}-\hat{z})}\,\ln\left(\frac{\hat{z}}{\hat{z}_o}\right)d\hat{z}$$

for convex downward (26b)

where $\hat{\varepsilon} = \varepsilon/c$; $\hat{\varepsilon} = \zeta\hat{d}$ if $\zeta\hat{d} > \hat{z}_o$; and $\hat{\varepsilon} = \hat{z}_o$ if $\zeta\hat{d} \le \hat{z}_o$ [Figure 3(b)]. The Simpson's rule is used to solve (26a) and (26b).

Results

As the lift coefficient C_L for shells is not known, the model is required to be calibrated extensively. The experimental data of incipient motion of shells are used to calibrate (22), making C_L a free parameter. The variation of estimated C_L with β is shown in Figure 4. As it is difficult to find a relationship between C_L and β from Figure 4, the average values of C_L, obtained as 0.206 and 0.953 in convex upward and downward conditions, respectively, are used for the computational purposes.

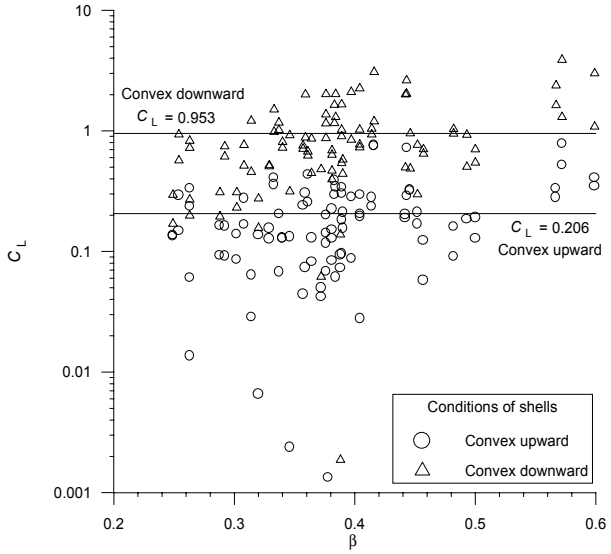

Figure 4. Variation of C_L with β in convex upward and downward conditions.

The equations developed in the preceding sections were used to provide a solution for $\hat{\tau}_o$ for incipient motion of shells. The comparisons of the values of $\hat{\tau}_o$ obtained using present model with the experimental data in convex upward and downward conditions are shown in Figure 5. The values of correlation coefficients between experimentally obtained and computed $\hat{\tau}_o$ in convex upward and downward conditions are 0.685 and 0.583, respectively. The model slightly underestimates the experimental results in convex downward condition. Nevertheless, the present model does a satisfactory job of estimating $\hat{\tau}_o$ with the experimental data on horizontal bed.

Conclusions

The incipient motion of bivalve shells on a horizontal sand bed, under a unidirectional flow of water, has been modeled from the basic concept of hydro-dynamics, including the effect of turbulent fluctuations. The present model agrees satisfactorily with the experimental data of incipient motion of shells in convex upward and downward conditions.

Acknowledgments

Thank are due to Bimalendu Dey for his advice on the presentation of the manuscript.

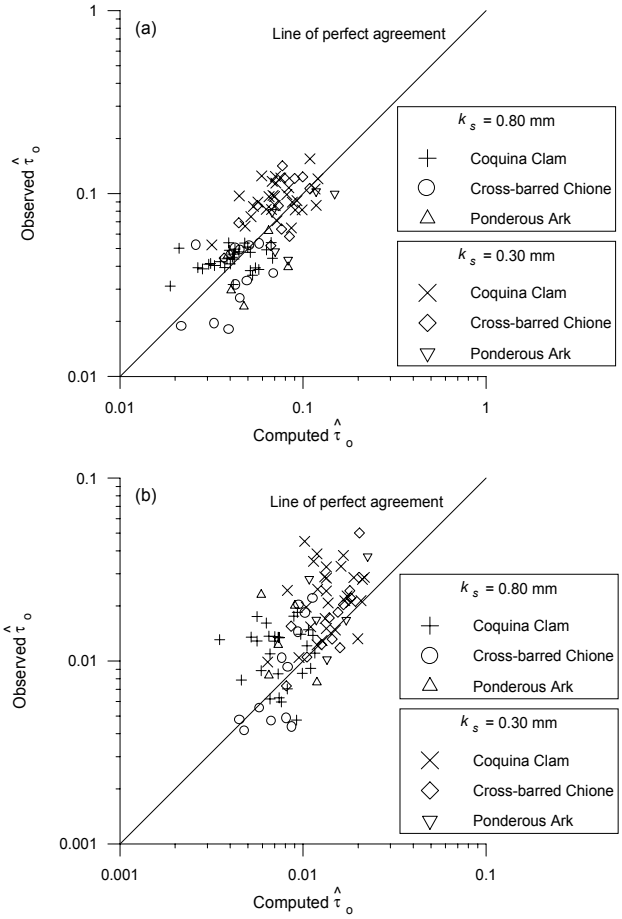

Figure 5. Comparison of the values of $\hat{\tau}_o$ obtained using present model with the experimental data for (a) convex upward and (b) convex downward conditions.

References

[1] Alger, G. R. & Simons, D. B., Fall Velocity of Irregular Shaped Particles, *J. Hydr. Div.*, ASCE, **94**, 1968, 721-737.

[2] Dey, S., Sediment Threshold, *Appl. Math. Modelling*, **23**, 1999, 399-417.

[3] Dey, S. & Bose, S. K., Bed Shear in Equilibrium Scour around a Circular Cylinder Embedded in a Loose Bed, *Appl. Math. Modelling*, **18**, 1994, 265-273.

[4] Dey, S. & Debnath, K., Influence of Streamwise Bed Slope on Sediment Threshold under Stream Flow, *J. Irrig. and Drain. Engrg.*, ASCE, **126**, 2000, 255-263.

[5] Dey, S. & Debnath, K., Sediment pickup on streamwise sloping beds, *J. Irrig. and Drain. Engrg.*, ASCE, **127**, 2001, 39-43.

[6] Dey, S., Dey Sarker, H. K. & Debnath, K., Sediment Threshold under Stream Flow on Horizontal and Sloping Beds, *J. Engrg. Mech.*, ASCE, **125**, 1999, 545-553.

[7] Keshavarzy, A. & Ball, J. E., The Influence of the Turbulent Shear Stress on the Initiation of Sediment Motion in an Open Channel Flow, *Proc. VII IAHR Int. Symp. Stochastic Hydr. 96*, 1996, 191-197.

[8] Mehta, A. J., Lee, J. & Christensen, B. A., Fall Velocity of Shells as Coastal Sediment, *J. Hydr. Div.*, ASCE, **106**, 1980, 1727-1744.

[9] Vanoni, V. A., Sedimentation Engineering, *ASCE Manual No. 54*, 1975.